MRS Advances (2025) 10:1036–1045
https://doi.org/10.1557/s43580-025-01244-5

ORIGINAL PAPER

Optimising synthesis conditions of PANI-NSA nanotubes for chromium removal

Nina Swart[1] · Luca Lohrentz[1] · Hendrik Brink[1]

Received: 28 January 2025 / Accepted: 10 March 2025 / Published online: 24 March 2025

Abstract

Polyaniline-naphthalene-sulfonic acid (PANI-NSA) nanotubes were synthesized and evaluated in this preliminary study for Cr(VI) removal from synthetic wastewater. SEM analysis showed that optimized synthesis conditions produced uniform nanotubes with additional surface spheres, potentially enhancing adsorption performance. Adsorption isotherms (Redlich-Peterson and Langmuir models) suggested a monolayer adsorption mechanism, while kinetic studies (Elovich and Wang two-phase models) indicated chemisorption-driven, diffusion-controlled adsorption. To explore the influence of synthesis conditions, temperature and water volume (as reaction eluent) were varied. PANI-NSA synthesized at 5 °C with 80 mL of water (more dilute) had an adsorption capacity of 374.9 mg g^{-1} (66.72% removal), increasing to 438.2 mg g^{-1} (79.28% removal) at 15 °C with 20 mL of water (i.e. more concentrated). While these results highlight promising trends, further detailed characterization and adsorption optimization studies are required to fully assess scalability and long-term application in industrial Cr(VI) remediation.

Introduction

The presence of heavy metal contaminants in water poses a significant threat to human health due to their tendency to accumulate in both the environment and the human body [1]. These metals are often released into the environment through industrial activities such as mining, manufacturing, and pesticide use. Hexavalent chromium, Cr(VI), is a toxic, carcinogenic heavy metal that is often released as an industrial pollutant [2]. Exposure to Cr(VI) can lead to skin irritation, lung cancer, and digestive problems [3]. In contrast, trivalent chromium, Cr(III), is an essential micro-nutrient that aids in the regulation of blood sugar levels and the transportation of glucose [3]. Therefore, the efficient removal of Cr(VI) from water sources remains a critical challenge in environmental engineering.

Several physical, biological, and chemical methods have been developed to remove heavy metals from water [4]. These include ion exchange, bioremediation, coagulation, evaporation, and adsorption. While these methods have been widely applied, they each suffer from specific limitations that hinder their effectiveness, particularly in large-scale or cost-sensitive applications [5]. Ion exchange is an effective method for removing metal ions from aqueous solutions, but it requires high operational costs and frequent regeneration of ion-exchange resins, which can generate secondary waste that requires additional treatment [6]. Bioremediation offers a sustainable approach to Cr(VI) removal, utilizing microorganisms such as *Pseudomonas* and *Bacillus* species to enzymatically reduce toxic Cr(VI) to the less harmful Cr(III), though challenges related to microbial tolerance and scalability remain [7]. Coagulation and precipitation are commonly employed for metal removal, using agents like ferric chloride or lime to facilitate metal precipitation. However, this approach is highly pH-dependent, generates large volumes of sludge that require disposal, and can lead to secondary contamination issues if not managed properly [8]. Evaporation and membrane-based separation processes, such as reverse osmosis, can achieve high removal efficiencies. However, they require significant energy input and suffer from membrane fouling issues, making them less economically viable for widespread industrial applications [9]. Due to these challenges, adsorption has emerged as one of the most promising techniques for heavy metal removal,

Nina Swart, Luca Lohrentz and Hendrik Brink have contributed equally to this work.

✉ Hendrik Brink
deon.brink@up.ac.za

[1] Department of Chemical Engineering, University of Pretoria, Roper Street, Pretoria 0083, Gauteng, South Africa

offering cost-effectiveness, high efficiency, and reusability when suitable adsorbents are employed [4].

Adsorption is a widely employed water treatment technique that involves the transfer of metal ions from aqueous solutions onto the surface of an adsorbent, offering a simple, cost-effective, and scalable remediation strategy [5]. Various nanomaterials, including carbon nanotubes, graphene, and metal oxide nanoparticles, have been extensively studied for their adsorption capabilities, as they provide high surface area and functionalized adsorption sites that enhance metal uptake [10, 11]. Among these materials, zero-valent-nickel-coated polyaniline-naphthalene-sulfonic acid (PANI-NSA@Ni^0) has shown great potential for the removal of heavy metals such as Cr(VI) [12] and lead [13]. However, studies indicate that Cr(VI) adsorption capacity using PANI-NSA@Ni^0 decreases by up to 88% after multiple adsorption–desorption cycles, requiring costly chemical re-doping to maintain performance [14]. This highlights the need to optimize PANI-NSA synthesis without nickel coating, improving adsorption efficiency and long-term stability while maintaining a more economically viable and sustainable approach.

The optimization of PANI-NSA synthesis is crucial, as current methods suffer from temperature and rate limitations that impact polymerization efficiency, nanotube morphology, and adsorption site distribution [15, 16]. This study serves as a preliminary exploration of how synthesis parameters influence the adsorption performance of PANI-NSA nanotubes, with a focus on optimizing temperature and water volume to enhance structural properties and adsorption efficiency. To ensure that adsorption performance variations arise solely from differences in material properties rather than adsorption process parameters, a constant adsorbent dosage was maintained throughout the experiments.

To assess the impact of synthesis modifications, adsorption isotherm modelling, kinetic analysis, and morphological characterization via scanning electron microscopy (SEM) were conducted. However, a more comprehensive understanding of the material's structural and chemical attributes—through BET surface area analysis, X-ray diffraction (XRD), and X-ray photoelectron spectroscopy (XPS)—remains necessary to elucidate the mechanisms governing adsorption at optimal synthesis conditions. Additionally, adsorption process optimization, including variations in adsorbent mass, contact time, and solution chemistry, will be addressed in future studies. This staged research approach ensures that the fundamental physicochemical properties of PANI-NSA nanotubes are well understood before advancing to process optimization for practical Cr(VI) remediation. The findings presented here provide key insights into the relationship between synthesis conditions and adsorption performance, laying the groundwork for subsequent studies aimed at maximizing the material's potential for industrial-scale applications.

Materials and methods

Materials

The materials required for the synthesis of PANI-NSA are ammonium persulfate, naphthalene-2-sulfonic acid, and aniline (99%). These materials were obtained from Sigma-Aldrich, USA. The additional materials required for analysis were analytical grade 1 M solutions of NaOH and HCl to be used for adjusting the pH, and 1, 5-Diphenylcarbazide (DPC) for analysing the absorbance of the chromium solution after adsorption. Deionized water was used in all experiments.

Standard PANI-NSA synthesis

PANI-NSA is formed rapidly via a chemical oxidative polymerisation reaction [12]. To synthesise the PANI-NSA, 0.208 g of naphthalene-2-sulfonic acid was added to 80 mL deionized water, after which 0.2 mL of aniline was added. This mixture was then placed in an ice bath to maintain the temperature between 0 and 5 °C and stirred for 30 min at 300 rpm using a magnetic stirrer. After 30 min, 0.456 g of ammonium persulfate (APS) dissolved in 10 mL of deionized water was added to the mixture, which was then stirred for an additional minute. The final mixture was left undisturbed at a temperature between 0 and 5 °C for 24 h to ensure sufficient time for complete polymerisation. Finally, the mixture was filtered, washed with deionised water, and vacuum dried at 60 °C for another 24 h [12, 14].

Varying synthesis temperature

The relationship between synthesis temperature and nanocomposite efficiency was investigated by modifying the reaction temperature while keeping all other synthesis parameters constant. The selected temperature range (10 °C, 15 °C, 20 °C, and 25 °C) was chosen based on previous studies demonstrating that temperature influences polymerization kinetics, nanotube formation, and adsorption site availability [15]. Lower temperatures ($\leq$ 10 °C) typically slow polymerization, leading to longer, more defined nanotubes with fewer defects, while higher temperatures ($\geq$ 25 °C) can accelerate polymerization, resulting in aggregation, overgrowth, and reduced surface accessibility [15].

To systematically evaluate these effects, PANI-NSA nanotubes were synthesized at 10 °C, 15 °C, 20 °C, and 25 °C using a temperature-controlled cooling bath, following the synthesis procedure described in Sect. 2.2. This approach allows for analysing the impact of temperature on morphological properties and adsorption performance, ensuring that variations in Cr(VI) removal efficiency can be attributed to structural differences induced by polymerization conditions.

Effect of reagent concentrations on synthesis and material Properties

The concentrations of the reagents during synthesis were modified by varying the amount of water used during synthesis. This approach follows chemical engineering principles for batch reactor systems, where varying the reaction medium volume affects the local concentration of reactants, influencing the morphology and adsorption performance of the final material [17, 18].

The synthesis procedure remained unchanged except for adjustments in water volume:

- 40 mL of deionized water instead of 80 mL, with 5 mL for APS dissolution.
- 20 mL of deionized water, with 2.5 mL for APS dissolution.

This method allows indirect assessment of the impact of adsorbent concentration on adsorption performance, aligning with reaction engineering principles while maintaining consistency in synthesis conditions.

Influence of pH on adsorption behaviour

The influence of solution pH on the adsorption behaviour of PANI-NSA nanotubes was evaluated to assess the effect of surface charge interactions on Cr(VI) removal. Since adsorption efficiency is strongly dependent on electrostatic interactions, and polyaniline-based materials typically exhibit a point-of-zero-charge (PZC) around pH 4.44 [14], it is crucial to determine how pH variations impact adsorption performance. The point-of-zero charge (PZC) refers to the pH at which the total positive and negative charges on the surface of the adsorbent are balanced [19]. Below this point, the surface carries a net positive charge, facilitating adsorption of anionic species such as Cr(VI), whereas at higher pH values, the surface becomes negatively charged, leading to electrostatic repulsion and decreased adsorption efficiency. By understanding this behaviour, we can establish a baseline for how synthesis modifications influence the material's adsorption characteristics under environmentally relevant conditions, without optimizing adsorption conditions in this preliminary study.

Batch adsorption experiments were conducted at pH values ranging from 2 to 11 to evaluate how the synthesized nanocomposite interacts with Cr(VI) across different pH conditions. The initial pH of 50 mL Cr(VI) solutions (100 mg L^{-1}) was adjusted using 0.1 M HCl or NaOH before adding 0.02 g of adsorbent. The solutions were stirred for 24 h to reach equilibrium, after which the final Cr(VI) concentration was measured using UV–Vis spectrophotometry at 540 nm.

Adsorption experiments

Batch adsorption experiments were conducted to determine the adsorption capacity of the nanocomposite. In the experiment, a 1000 ppm hexavalent chromium stock solution was diluted to 200 ppm in 25 mL glass bottles. 0.015 g of PANI-NSA nanocomposite was then added to the glass bottles and the pH adjusted to the experimentally determined optimal operating pH. After leaving the bottles in a shaker set to 200 rpm for 24 h, the residual chromium concentration in each bottle was measured using a spectrophotometer at 540 nm (VWR UV-1600PC) [12]. From these results, the percentage chromium removal was determined using Eq. 1.

$$\%removal = \frac{100\left(C_o - C_e\right)}{C_o} \tag{1}$$

With C_o the initial chromium concentration, and C_e the equilibrium chromium concentration.

Adsorption isotherms

Adsorption isotherms are used to explain how much of a substance gets adsorbed at different concentrations. The isotherm data were obtained for the PANI-NSA synthesised at both the normal and the optimised conditions and compared to one another. To obtain the isotherm data, 25 mL glass bottles were prepared in which the initial chromium concentration was varied from 20 to 400 ppm. The pH for each bottle was adjusted to the experimentally obtained optimal pH value and 0.015 g of the nanocomposite was added to each bottle [12]. The solutions were left in a shaker set to 200 rpm for 24 h. Thereafter, the final chromium was recorded, and the percentage chromium removal calculated. The isotherm data was modelled and compared by using the single-site (Eq. 2), dual-site (Eq. 4), Freundlich (Eq. 3), and Redlich-Peterson (Eq. 5) isotherms [20, 21]. These models characterize how an adsorbate interacts with an adsorbent at equilibrium and help in understanding adsorption mechanisms.

$$q_e = \frac{q_{max} K_L C_e}{1 + K_L C_e} \tag{2}$$

$$q_e = b C_e^{\frac{1}{n}} \tag{3}$$

$$q_e = \frac{q_{max,1} K_{L1} C_e}{1 + K_{L1} C_e} + \frac{q_{max,2} K_{L2} C_e}{1 + K_{L2} C_e} \tag{4}$$

$$q_e = \frac{K_r C_e}{1 + a C_e^{\beta}} \tag{5}$$

In these equations, q_e represents the equilibrium adsorption capacity, which is the amount of adsorbate retained per unit mass of adsorbent at equilibrium. The variable C_e denotes the equilibrium concentration of the adsorbate in solution. The parameters q_{max} and K_L appear in multiple equations and represent the maximum adsorption capacity and the Langmuir equilibrium constant, respectively, which describe the strength of adsorption interactions. Equation (2) represents the Langmuir isotherm, assuming monolayer adsorption onto a homogeneous surface. Equation (3) corresponds to the Freundlich isotherm, where b is the adsorption capacity constant and $1/n$ indicates surface heterogeneity. Equation (4) is the dual-site Langmuir isotherm, incorporating two different adsorption sites with distinct equilibrium constants (K_{L1}, K_{L2}) and capacities (q_{max1}, q_{max2}). Finally, Eq. (5) represents the Redlich-Peterson isotherm, which blends Langmuir and Freundlich characteristics, where K_r is the isotherm constant, a is an empirical parameter, and β ($0 < \beta \leq 1$) describes deviation from ideal monolayer adsorption. These models collectively help in understanding adsorption mechanisms and optimizing material performance in adsorption-based applications.

Adsorption kinetics

The adsorption kinetics of the normal nanocomposite was compared to that of the optimal nanocomposite. The kinetics were compared at 25 °C by adding 0.3 g of PANI-NSA to 500 mL of a 50 mg/L chromium solution [12]. The kinetic data was obtained by removing 5 mL of the chromium solution at regular time intervals until equilibrium was reached. The 5 mL samples were analysed using a spectrophotometer (VWR UV-1600PC). The kinetic models that were used for this comparison are the Wang Two-Phase (Eq. 6), Elovich (Eq. 7), Pseudo Second-Order (Eq. 8), and Pseudo First-Order (Eq. 9) kinetic models [21–23]. These models describe how adsorption progresses over time and provide insights into the adsorption mechanism.

$$q_t = q_{e,slow}\left(1 - e^{-k_{slow}t}\right) + \left(q_e - q_{e,slow}\right)\left(1 - e^{-k_{fast}t}\right) \tag{6}$$

$$q_t = \frac{1}{\beta}\ln(1 - \alpha\beta t) \tag{7}$$

$$\frac{dq_t}{dt} = k_1\left(q_e - q_t\right)^2 \tag{8}$$

$$\frac{dq_t}{dt} = k_1\left(q_e - q_t\right) \tag{9}$$

In all models, q_t represents the adsorption capacity at time t, while q_e denotes the equilibrium adsorption capacity. The Wang Two-Phase Model accounts for both fast and slow adsorption phases, where $q_{e,slow}$ represents the fraction of adsorption occurring in the slow phase, with k_{slow} and k_{fast} as the corresponding rate constants. The Elovich Model describes chemisorption kinetics, where α is the initial adsorption rate and β is the desorption constant [23]. The Pseudo-Second-Order Model assumes adsorption is controlled by surface reaction kinetics, with k_2 as the rate constant, and suggests that the adsorption rate is proportional to the square of the available adsorption sites. The Pseudo-First-Order Model assumes the adsorption rate is directly proportional to the difference between equilibrium and instantaneous adsorption, with k_1 as the rate constant. These models provide valuable insights into adsorption mechanisms and aid in optimizing material performance for pollutant removal applications.

Morphological characterisation

The morphology and size of the synthesized PANI-NSA nanotubes were examined to assess the impact of varying synthesis conditions. Scanning electron microscopy (SEM) was conducted using a Zeiss Gemini Ultra Plus FEG Scanning Electron Microscope (Carl Zeiss, Germany) to capture high-resolution images of the materials. Samples were prepared by drop-casting the nanocomposite dispersion onto carbon-coated aluminium stubs, followed by drying at room temperature. Imaging was performed under high-vacuum conditions at an accelerating voltage of 2.00 kV, ensuring optimal contrast and resolution for observing nanotube formation and surface modifications.

Results and discussion

Effect of synthesis temperature on chromium removal and nanotube morphology

From Fig. 1a, it is evident that initially the Cr(VI) removal efficiency remained relatively stable with increasing synthesis temperature. The highest chromium removal was achieved at 15 °C, after which the removal efficiency dropped significantly between 15 °C and 25 °C. This trend suggests that the synthesis conditions influence the structural characteristics of the nanotubes, which in turn impact adsorption performance.

The morphology of the PANI-NSA nanotubes synthesized at different temperatures, as shown in Figs. 1b–d, provides insights into the structural changes responsible for these adsorption trends. At 5 °C (Fig. 1b), the nanotubes appear well-defined and sparsely distributed, with minimal aggregation and relatively smooth surfaces. This suggests that lower synthesis temperatures limit polymerization,

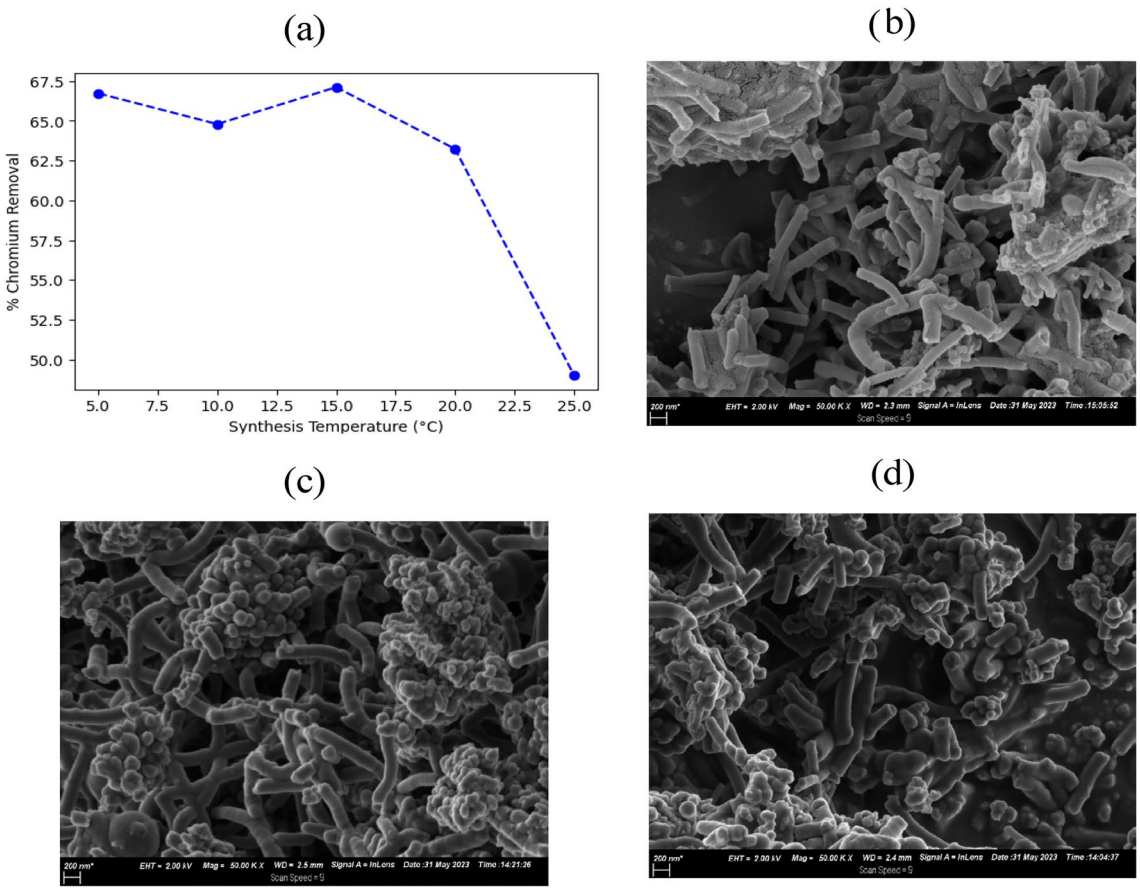

Fig. 1 Effect of synthesis temperature on **a** Cr(VI) removal efficiency and (**b–d**) morphological changes at varying synthesis temperatures: **b** 5 °C, **c** 15 °C, and **d** 25 °C, respectively

resulting in nanotubes with relatively simple morphology and fewer structural defects. The well-separated nanotube formation may contribute to stable adsorption performance but lacks the increased clustering that enhances surface interactions [15].

At 15 °C (Fig. 1c, optimized conditions), the nanotubes remain uniform in size but exhibit increased clustering and the formation of additional spherical structures on their surfaces [15]. These spherical formations may be polymerized byproducts or functionalized adsorption sites, contributing to higher adsorption efficiency by increasing available surface interactions. The clustering effect suggests a more interconnected nanotube network, which could enhance adsorbate diffusion and surface interactions, leading to the highest Cr(VI) removal observed at this temperature.

However, at 25 °C (Fig. 1d), polymerization appears excessive, leading to the formation of larger, less-defined aggregates. The nanotube structure is partially lost due to overgrowth, with increased agglomeration reducing the number of well-formed nanotubes [15]. This structural collapse likely decreases the available surface area and obstructs active adsorption sites, negatively impacting adsorption capacity. The observed drop in Cr(VI) removal efficiency above 15 °C aligns with this loss of structural integrity and reduced accessibility of adsorption sites.

These findings confirm that synthesis temperature has a direct impact on nanotube morphology, which in turn determines the adsorption performance of the material. The observed trend suggests that 15 °C is the optimal synthesis temperature for achieving a balance between polymerization efficiency, structural integrity, and surface accessibility, leading to enhanced Cr(VI) adsorption performance. Future studies incorporating BET surface area analysis and pore size distribution measurements will provide further insights into how temperature-induced morphological changes impact adsorption efficiency.

Effect of synthesis water volume on nanotube morphology and chromium adsorption

The adsorption capacity of the PANI-NSA nanocomposite increased as the amount of water used in synthesis

decreased, as shown in Table S1. Despite variations in water volume, the total mass of the synthesized adsorbent remained approximately 0.15 g, indicating that the synthesis reaction proceeded to completion across all conditions. This suggests that the observed changes in adsorption performance were primarily due to morphological differences in the synthesized material, rather than variations in total yield.

The morphology of the nanocomposites, as illustrated in Fig. 2a–c, shows distinct structural differences influenced by the amount of water used during synthesis. When 80 mL of water was used (Fig. 2a, standard condition), the nanotubes appeared relatively well-formed but loosely distributed, indicating a more dispersed polymer network. Reducing the water volume to 40 mL (Fig. 2b) led to increased clustering of nanotubes, while further reduction to 20 mL (Fig. 2c) resulted in denser nanotube networks with additional spherical formations on the surface. These morphological changes suggest that higher reactant concentration (lower water volume) enhances polymerization, leading to a more compact structure and possibly a greater number of active adsorption sites [16].

The increase in adsorption capacity with decreasing water volume can be attributed to localized reactant concentration effects during synthesis, which influence the morphology, surface area, and available adsorption sites of the final material. According to chemical reaction engineering principles [17, 18], in a batch polymerization system, varying the reaction medium volume directly affects the concentration of reactants, altering the growth kinetics of the polymer network. As the water volume decreased, the localized concentration of aniline, ammonium persulfate (APS), and naphthalene-2-sulfonic acid increased, resulting in denser polymerization and enhanced nanotube formation. This structural change likely led to an increased number of active adsorption sites, thereby improving Cr(VI) removal efficiency.

The synthesis conditions likely influenced the surface charge distribution and porosity of the adsorbent, enhancing chromium adsorption. The observed clustering and densification of nanotube structures at lower water volumes suggest an increased number of adsorption sites, improving electrostatic interactions with Cr(VI) species. Studies on PANI synthesis have shown that reagent concentrations significantly affect morphology, yield, and electrical properties. The oxidant-to-monomer ratio ([O]/[M]) is particularly crucial for conductivity, with an optimal ratio (~0.4) enhancing conductivity, while further increases disrupt morphology and nucleation sites [16]. Similarly, higher dopant concentrations promote well-defined nanofibers and improved electrical properties [24]. Ddditionally, oxidant concentration and stirring rate play key roles in polymerization efficiency, though they have minimal impact on thermal stability [25]. These factors collectively influence adsorbent structure, which in turn affects adsorption performance. Future studies employing BET surface area analysis and porosity measurements will provide further insight into these effects and confirm whether the increased adsorption capacity is directly related to surface area improvements.

These observations, coupled with the results from Sect. 3.1, confirm that 15 °C and 20 mL of water represent the optimal synthesis conditions (summarised in Table S2), as they produce nanotubes with a balance between structural integrity and surface accessibility, leading to improved Cr(VI) adsorption performance. To gain a deeper understanding of the structural properties, X-ray diffraction (XRD) and X-ray photoelectron spectroscopy (XPS) analyses will be conducted to determine crystallinity and surface chemistry, further elucidating the relationship between morphology and adsorption efficiency. These findings will inform subsequent optimization efforts, ensuring that the material design is tailored for scalability and practical applications in Cr(VI) remediation.

Effect of pH on adsorption performance

The adsorption efficiency of PANI-NSA nanotubes was strongly influenced by solution pH, as shown in Figure S1. The highest chromium removal efficiency of 65.11% was obtained at pH 2, followed by 51.96% at pH 3. These results confirm that chromium adsorption is promoted below the

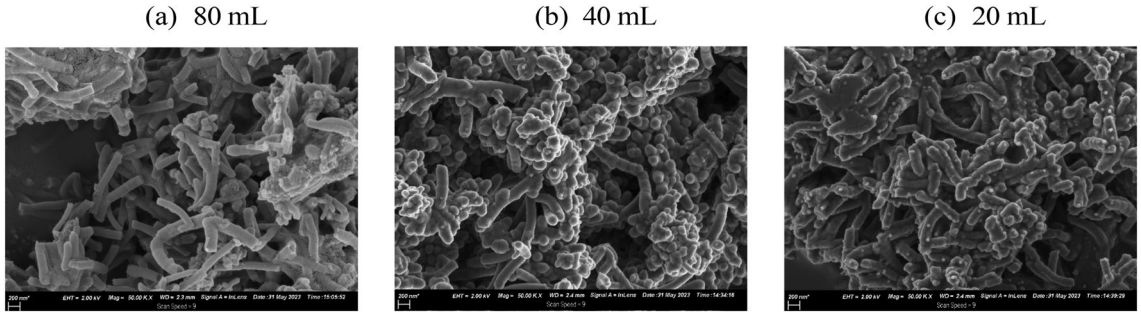

Fig. 2 Morphology at varying synthesis water volumes: **a** 80 mL (standard condition), **b** 40 mL, **c** 20 mL

point-of-zero-charge (PZC), where the adsorbent surface is positively charged, enhancing electrostatic attraction with negatively charged Cr(VI) species ($HCrO_4^-$, $Cr_2O_7^{2-}$). The PZC for PANI-NSA is reported as pH 4.44 [14], supporting the observed trend where adsorption is most effective at pH values below this threshold.

To ensure maximum chromium adsorption during batch experiments, the operating pH was maintained at pH 2, as it provided the highest adsorption efficiency. This pH dependence is consistent with previously reported electrostatic adsorption mechanisms for polyaniline-based materials, reinforcing the role of surface charge in Cr(VI) removal.

Adsorption isotherms

Adsorption isotherms characterize the interaction between the adsorbent and the adsorbate, providing insights into the adsorption capacity and surface properties of the nanocomposites. The isotherm data can be used to calculate and compare the maximum adsorption capacity (q_m) of the materials under different synthesis conditions. The maximum adsorption capacity of the PANI-NSA nanocomposite synthesized under normal conditions was calculated as 347.9 mg g^{-1}, which increased to 438.2 mg g^{-1} under optimized synthesis conditions. This improvement suggests that modifications in synthesis parameters significantly enhance the adsorption efficiency of the material.

Figure 3a shows the fit obtained from the Single-Site Langmuir (SS Langmuir), Dual-Site Langmuir (DS Langmuir), Redlich-Peterson, and Freundlich models for the nanocomposite synthesized at normal conditions, while Fig. 3b presents the corresponding fits for the optimized nanocomposite. The best-fit isotherm parameters are provided in Table S3.

For the nanocomposite synthesized under optimized conditions, the contribution of the second adsorption site in the dual-site Langmuir model was negligible, as indicated by the small q_{m2} value. In this case, both the Dual-Site Langmuir and Redlich-Peterson models simplified to the Single-Site Langmuir model, indicating that adsorption occurs predominantly on a single type of binding site. The small K_{L1} value further suggests that adsorption on this site is reversible.

In contrast, for the nanocomposite synthesized under normal conditions, the effect of the second site was significantly more pronounced. Both adsorption sites exhibited reversible adsorption, as indicated by the small K_{L1} and K_{L2} values. By analysing the R^2 values from Table S3, it is evident that the Dual-Site Langmuir and Redlich-Peterson models provide a more accurate representation of the adsorption behaviour than the Single-Site Langmuir model. The Dual-Site Langmuir model provided the best fit for the nanocomposite synthesized under normal conditions, suggesting that a heterogeneous adsorption mechanism dominates in this case, whereas a monolayer adsorption mechanism is preferred under optimized synthesis conditions [12].

These findings indicate that synthesis modifications influence not only adsorption capacity but also adsorption site distribution, highlighting the importance of optimizing synthesis conditions to enhance the efficiency and predictability of the adsorption process.

Adsorption kinetics

The adsorption kinetics of the PANI-NSA nanocomposites synthesized under normal and optimized conditions were evaluated using pseudo-first-order (PFO), pseudo-second-order (PSO), Elovich, and Wang two-phase models. These kinetic models provide insights into the adsorption mechanisms and rate-controlling steps, which are critical for understanding whether modifications in synthesis conditions affect the adsorbent's overall performance. Ensuring that a change in synthesis temperature or reactant concentration does not significantly alter adsorption kinetics is essential for maintaining the material's practical applicability.

As detailed in Sect. 2.8, kinetic experiments were conducted using a 50 ppm Cr(VI) solution, and the adsorption performance of the nanocomposites was compared. The equilibrium adsorption capacity (q_e) for PANI-NSA synthesized under normal conditions was 57.53 mg g^{-1}, whereas for the PANI-NSA synthesized under optimized conditions, the capacity increased slightly to 59.37 mg g^{-1}. The adsorption behaviour was modelled using the kinetic equations, and the corresponding fits are shown in Fig. 4a (normal synthesis conditions) and Fig. 4b (optimized synthesis conditions). The best-fit parameters are summarized in Table S4.

From the R^2-values in Table S4, it is evident that the pseudo-first-order and pseudo-second-order models are less suitable for describing the adsorption process, as they do not adequately capture the multi-step nature of Cr(VI) adsorption onto the nanocomposites. Instead, the Elovich and Wang two-phase models provided a significantly better fit to the experimental data, indicating that the adsorption process likely involves both chemisorption and surface diffusion mechanisms [23].

The Wang two-phase model demonstrated the best overall fit ($R^2 = 0.9738$ for optimized conditions, 0.9670 for normal conditions), suggesting that adsorption occurs in two distinct stages [23]:

1. An initial rapid phase, where a large fraction of Cr(VI) ions are adsorbed onto the available active sites of the nanocomposite surface. The fast adsorption rate constant (k_{fast}) increased from 0.6875 to 0.8078, indicating

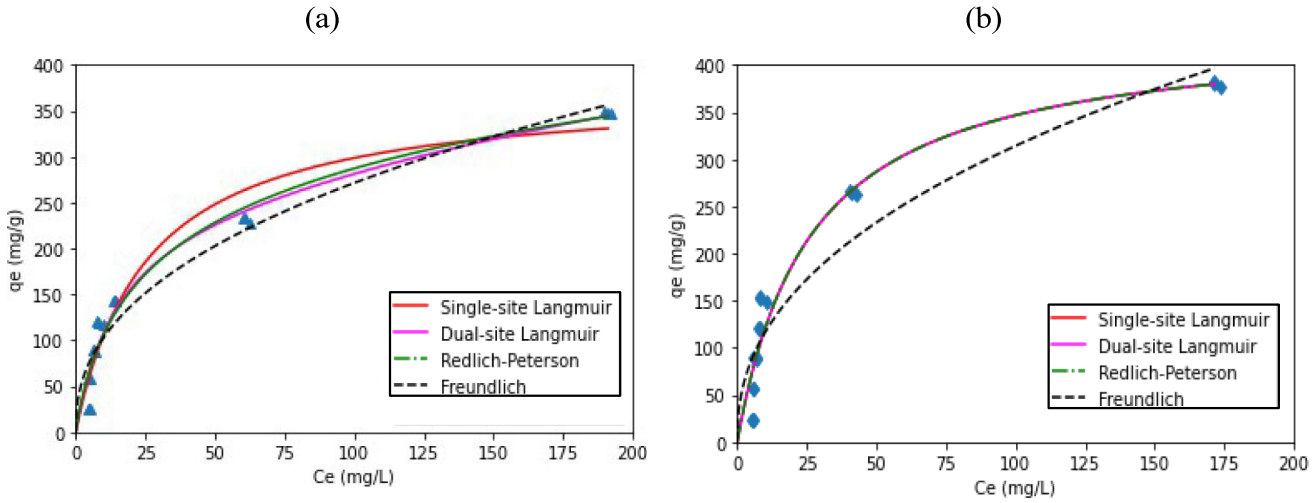

Fig. 3 **a** Isotherms for nanocomposite formed at standard conditions, **b** Isotherms for nanocomposite formed at optimised conditions

improved adsorption kinetics under optimized conditions.

2. A slower diffusion-controlled phase, where adsorption continues but at a reduced rate due to the progressive occupation of adsorption sites. The slow adsorption rate constant (k_{slow}) increased from 0.00961 to 0.01631, suggesting that the optimized material retained adsorption efficiency even in the slower phase.

The Elovich model also provided a good fit ($R^2 = 0.9582$ for optimized conditions, 0.9624 for normal conditions), further supporting the presence of chemisorption-driven adsorption mechanisms. The decrease in the β parameter (from 0.1503 to 0.1172) suggests that the optimized material required less activation energy for adsorption, which could contribute to the slight increase in adsorption capacity [23].

The significant increase in both fast and slow rate constants, as well as the equilibrium adsorption capacity (q_e) in the Wang model, increasing from 57.53 to 59.37 mg g^{-1}, confirms that optimized synthesis conditions not only enhanced adsorption capacity but also significantly promoted adsorption kinetics. The increased rate constants indicate that the interaction between Cr(VI) ions and the nanocomposite surface became more efficient, likely due to improved surface accessibility, increased availability of adsorption sites, and enhanced charge distribution. These enhancements suggest that the nanocomposite synthesized under optimized conditions offers superior performance in both adsorption rate and capacity, making it a more effective adsorbent for Cr(VI) removal.

These findings highlight that optimized synthesis does not merely increase adsorption capacity but actively improves adsorption kinetics, allowing for faster and more effective removal of Cr(VI). Future studies incorporating diffusion and mass transfer modelling will further elucidate the adsorption pathways and transport limitations of the synthesized nanocomposites, providing deeper insights into their practical application for water treatment.

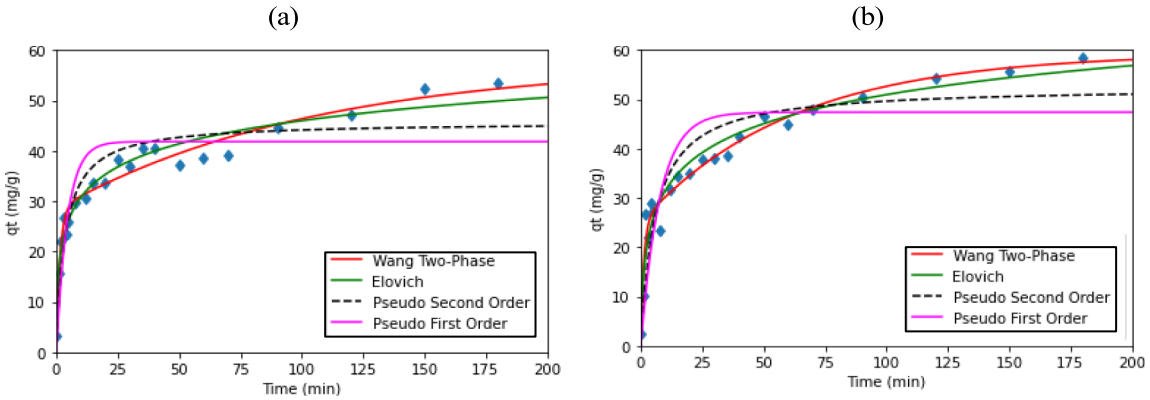

Fig. 4 **a** Kinetics at 50 ppm solution for nanocomposite formed at normal conditions, **b** Kinetics at 50 ppm solution for nanocomposite formed at optimised conditions

Comparison with literature

The adsorption capacity of PANI-NSA synthesized under optimized conditions (438.2 mg g^{-1}) in this study is comparable to or exceeds many previously reported PANI-based adsorbents for Cr(VI) removal (see Table S5). For instance, PANI-Fe/OMC composite achieved 172.3 mg g^{-1} due to the synergistic effects of Fe and ordered mesoporous carbon [26], while PANI confined in SC/HA/PVA hydrogel exhibited an exceptionally high capacity of 1180.97 mg g^{-1}, attributed to enhanced surface area and functional group availability [27]. The PANI-Macadamia nutshell composite (384.6 mg g^{-1}) [28] and PANI/PVA/AFL gel beads (51.5 mg g^{-1}) [29] further demonstrate the variability in Cr(VI) adsorption efficiency depending on material composition and synthesis modifications. The adsorption performance of PANI-NSA in this study aligns well with high-performing composites, emphasizing that synthesis optimization without additional dopants or metal functionalization can significantly improve adsorption efficiency. These findings support the potential scalability of optimized PANI-NSA nanotubes for Cr(VI) remediation, with future work required to evaluate surface area contributions (BET) and adsorption site interactions (XPS, FTIR) to further contextualize its adsorption mechanisms.

Conclusion and recommendations

This study demonstrated that optimizing the synthesis conditions of PANI-NSA nanocomposites significantly enhances their Cr(VI) adsorption performance. By modifying the synthesis temperature and reactant concentration, the structural and adsorption properties of the nanocomposite were improved. The optimal synthesis conditions were determined to be 15 °C and 20 mL of deionized water, while the optimal adsorption pH was found to be pH 2. Under these conditions, the Cr(VI) removal efficiency increased from 66.72% (normal synthesis conditions) to 79.28%, and the equilibrium adsorption capacity increased from 374.9 mg g^{-1} to 438.2 mg g^{-1}. Morphological analysis revealed that PANI-NSA synthesized under normal conditions formed long, thin nanotubes, whereas PANI-NSA synthesized under optimized conditions produced nanotubes of comparable size and thickness, but with additional spherical formations on their surfaces. These morphological changes suggest a possible increase in surface area, which could contribute to the enhanced adsorption performance observed at optimized synthesis conditions. However, it is recommended that BET surface area analysis be conducted to accurately quantify and compare the surface areas of both nanocomposites. Adsorption isotherm analysis revealed that the Redlich-Peterson and Langmuir models provided the best fit for both nanocomposites, indicating a monolayer adsorption process with potential heterogeneous interactions. Additionally, the adsorption kinetics were best described by the Elovich and Wang two-phase models, suggesting that the adsorption process is governed by chemisorption mechanisms and multi-step diffusion processes.

To further elucidate the Cr(VI) removal mechanism, X-ray Photoelectron Spectroscopy (XPS) and X-ray Diffraction (XRD) analyses should be performed. XPS is particularly useful for identifying surface interactions between Cr(VI) and the nanocomposite by detecting oxidation states and chemical bonding changes, which can confirm whether adsorption occurs via electrostatic attraction or redox transformation. XRD, on the other hand, provides information on crystalline phase changes, allowing for the identification of any structural modifications to PANI-NSA post-adsorption. These techniques have been widely applied in studies of heavy metal adsorption onto polymeric and nanostructured adsorbents and are well-suited for confirming the adsorption and possible reduction of Cr(VI) to Cr(III) on the nanocomposite surface [12–14, 21]. Additionally, the reusability and regeneration potential of the nanocomposite should be explored, as this would provide insight into the economic feasibility and sustainability of PANI-NSA for large-scale Cr(VI) remediation. Recovering and repurposing the adsorbed chromium for industrial applications, while enabling the repeated use of the nanocomposite as an adsorbent, could further enhance its practical applicability.

These findings provide a strong foundation for future research on the synthesis-adsorption relationship of PANI-NSA nanocomposites and highlight the importance of continued material optimization to improve Cr(VI) remediation efficiency.

Supplementary Information The online version contains supplementary material available at https://doi.org/10.1557/s43580-025-01244-5.

Author contributions These authors contributed equally to this work.

Funding Open access funding provided by University of Pretoria. The work was supported by the Austrian Federal Ministry of Education, Science and Research (BMBWF) through Austria's Agency for Education and Internationalization (OeAD) [Grant numbers: Africa UNINET P056 and P058 as well as APPEAR Project 341]. APPEAR is a program of the Austrian Development Organization.

Data availability The data will be made available upon request from the authors.

Materials availability Not applicable.

Code availability Not applicable.

Declarations

Conflict of interest The authors declare that they have no conflicts of interests.

Ethical approval Not applicable.

References

1. J. Briffa, E. Sinagra, R. Blundell, Heavy metal pollution in the environment and their toxicological effects on humans. Heliyon **6**, e04691 (2020)
2. M. Jashaid, A.A. Khan, K. Ahmed, M. Saleem, Heavy metal in drinking water, its effect on human health and its treatment techniques—a review. Int. J. Biosci. **12**, 223–240 (2018)
3. A. Monga, A.B. Fulke, D. Dasgupta, Recent developments in essentiality of trivalent chromium and toxicity of hexavalent chromium: Implications on human health and remediation strategies. J. Hazar. Mater. Adv. **7**, 100113 (2022)
4. G. Yu, X. Wang, J. Liu, P. Jiang, S. You, N. Ding, Q. Guo, F. Lin, Applications of nanomaterials for heavy metal removal from water and soil: a review. Sustainability **13**, 713 (2021)
5. F. Fu, Q. Wang, Removal of heavy metal ions from wastewaters: a review. J. Environ. Manage. **92**(3), 407–418 (2011)
6. E. Sgreccia, C. Rogalska, F.S. Gallardo Gonzalez, P. Prosposito, L. Burratti, P. Knauth, M.L. Di Vona, Heavy metal decontamination by ion exchange polymers for water purification: counterintuitive cation removal by an anion exchange polymer. J. Mater. Sci. **59**, 2776–2787 (2024)
7. M. Huang, X. Luo, Y. Shi et al., Mechanisms involving the facilitation of the remediation of Cr(VI) contaminated soil by bacteria-loaded biochar. Int. J. Environ. Res. **19**, 45 (2025). https://doi.org/10.1007/s41742-024-00717-z
8. F. Nyström, K. Nordqvist, I. Herrmann, A. Hedström, M. Viklander, Removal of metals and hydrocarbons from stormwater using coagulation and flocculation. Water Res. **182**, 115919 (2020)
9. S. Aziz, A.R. Mazhar, A. Ubaid, S.M.H. Shah, Y. Riaz, T. Talha, D.-W. Jung, A comprehensive review of membrane-based water filtration techniques. Appl. Water Sci. (2024). https://doi.org/10.1007/s13201-024-02226-y
10. S.S. Kerur, S. Bandekar, M.S. Hanagadakar, S.S. Nandi, G.M. Ratnamala, P.G. Hegde, Removal of hexavalent chromium-industry treated water and wastewater: a review. Mater. Today: Proc. **42**, 1112–1121 (2021)
11. N.A. Azeez, S.S. Dash, S.N. Gummadi, V.S. Deepa, Nano-remediation of toxic heavy metal contamination: hexavalent chromium (cr(vi)). Chemosphere **266**, 129204 (2021)
12. L. Lohrentz, M. Bhaumik, H.G. Brink, High-capacity adsorption of hexavalent chromium by a polyaniline-ni(0) nanocomposite adsorbent: Expanding the langmuir-hinshelwood kinetic model. J. Mol. Liquids **309**, 122931 (2023)
13. M. Bhaumik, C. Noubactep, V.K. Gupta, R.I. McCrindle, A. Maity, Polyaniline/Fe^0 composite nanofibres: an excellent adsorbent for the removal of arsenic from aqueous solutions. Chem. Eng. J. **271**, 135–146 (2015)
14. M. Bhaumik, A. Maity, H.G. Brink, Zero valent nickel nanoparticles decorated polyaniline nanotubes for the efficient removal of *Pb*(*II*) from aqueous solution: synthesis, characterization and mechanism investigation. Chem. Eng. J. **417**, 127910 (2021)
15. F. Yılmaz, Z. Küçükyavuz, The influence of polymerization temperature on structure and properties of polyaniline. e-Polymers (2009). https://doi.org/10.1515/epoly.2009.9.1.48
16. S. Ghanbari, S. Pourmahdian, Effect of synthesis parameters on electrical conductivity and morphological characteristics of pristine PANI and polyaniline-MWCNT nanocomposites. J. Mater. Sci. Mater. Electron. **34**, 1541 (2023). https://doi.org/10.1007/s10854-023-10875-z
17. Fogler, H. S. Elements of Chemical Reaction Engineering (5th ed.). Pearson (2016).
18. Levenspiel, O. Chemical Reaction Engineering (3rd ed.) Wiley (1999).
19. E.A. Al-Maliky, H.A. Gzar, M.G. Al-Azawy, Determination of point of zero charge (pzc) of concrete particles adsorbents. IOP Conf. Series: Mater. Sci. Eng. **1184**, 012004 (2021)
20. S. Kalam, S.A. Abu-Khamsin, M.S. Kamal, S. Patil, Surfactant adsorption isotherms: a review. ACS Omega **6**, 32342–32348 (2021)
21. J. Wang, Y. Wei, Z. Ma, Modified dual-site langmuir adsorption equilibrium models from a gcmc molecular simulation. Appl. Sci. **10**, 1311 (2020)
22. Z. Wang, J. Zhao, L. Song, H. Mashayekhi, B. Chefetz, B. Xing, Adsorption and desorption of phenanthrene on carbon nanotubes in simulated gastrointestinal fluids. Environ. Sci. Tech. **45**, 6018–6024 (2011)
23. L. Largitte, R. Pasquier, A review of the kinetics adsorption models and their application to the adsorption of lead by an activated carbon. Chem. Eng. Res. Des. **109**, 495–504 (2016)
24. F. Rezaei, N.P. Tavandashti, A.R. Zahedi, Morphology of polyaniline nanofibers synthesized under different conditions. Res. Chem. Intermed. **40**, 1233–1247 (2014). https://doi.org/10.1007/s11164-013-1035-1
25. M. Cortés, E. Sierra, Effect of synthesis parameters in polyaniline: influence on yield and thermal behavior. Polym. Bull. **56**, 37–45 (2006). https://doi.org/10.1007/s00289-005-0467-1
26. J. Wen, Y. Zhang, Y. Du, Effective removal of Cr(VI) in water by bulk-size polyaniline/polyvinyl alcohol/amyloid fibril composite beads. Water Sci. Technol. **88**(8), 1944–1956 (2023)
27. O.I. Adeiga, T. Velempini, K. Pillay, Polyaniline-decorated *Macadamia* nutshell composite: an adsorbent for the removal of highly toxic Cr(VI) and efficient catalytic activity of the spent adsorbent for reuse. Polym. Bull. **80**, 1951–1973 (2023). https://doi.org/10.1007/s00289-021-04009-w
28. G. Yang, L. Tang, Y. Cai, G. Zeng, P. Guo, G. Chen, Y. Zhou, J. Tang, J. Chen, W. Xiong, Effective removal of Cr(vi) through adsorption and reduction by magnetic mesoporous carbon incorporated with polyaniline. RSC Adv. **4**, 58362 (2014). https://doi.org/10.1039/C4RA08432B
29. X. Zhang, Y. Li, W. Zou et al., Sorption enhancement of Cr(VI) from aqueous solution by polyaniline confined in three-dimensional network of composite porous hydrogel. Environ. Sci. Pollut. Res. **30**, 92404–92416 (2023). https://doi.org/10.1007/s11356-023-28948-1